



Article

Critical Evaluation and Thermodynamic Optimization of the Cr–P and Cr–Fe–P Systems

Zhimin You ¹, Zhijie Lai ¹, Senlin Cui ², Zhouhua Jiang ^{1,*} and In-Ho Jung ^{3,*}

¹ School of Metallurgy, Northeastern University, No. 3–11, Wenhua Road, Heping District, Shenyang 110819, China; youzhimin@smm.neu.edu.cn (Z.Y.); 18040104585@163.com (Z.L.)

² School of Civil Aviation, Northwestern Polytechnical University, Xi'an 710072, China; pkbedu@nwpu.edu.cn

³ Department of Materials Science and Engineering, Research Institute of Advanced Materials (RIAM), Seoul National University, 1 Gwanak-ro, Gwanak-gu, Seoul 08826, Republic of Korea

* Correspondence: jiangzh@smm.neu.edu.cn (Z.J.); in-ho.jung@snu.ac.kr (I.-H.J.)

Abstract: Existing thermodynamic descriptions of the whole Cr–Fe–P system are insufficiently accurate for understanding the thermodynamic behavior of the Cr–Fe–P materials during the manufacturing process. To construct a more precise and consistent thermodynamic database of the Cr–Fe–P system, thermodynamic modeling of the Cr–P and Cr–Fe–P systems was conducted using the CALculation of PHase Diagrams (CALPHAD) approach based on critical evaluation of the experimental data. The modified quasichemical model and compound energy formalism were employed to describe the liquid and solid solutions, respectively. The Gibbs energies of stoichiometric compounds Cr₃P(s), Cr₂P(s), CrP(s), and CrP₂(s) were carefully determined based on reliable experimental data. The ternary (Cr,Fe)₃P, (Cr,Fe)₂P, and (Cr,Fe)P phosphides were modeled as solid solutions considering mutual substitution between Cr and Fe atoms. In addition, the phase equilibria of BCC_A2 and FCC_A1 solutions and the liquid phase of the ternary Cr–Fe–P system were also optimized for more accurate descriptions of existing phase equilibria and thermodynamic properties data. As an application of the present database, the experimentally unexplored thermodynamic properties and phase diagrams of the Cr–Fe–P system are predicted.

Keywords: thermodynamic modeling; Cr–P system; Cr–Fe–P system; thermodynamic properties; phase diagram



Citation: You, Z.; Lai, Z.; Cui, S.; Jiang, Z.; Jung, I.-H. Critical Evaluation and Thermodynamic Optimization of the Cr–P and Cr–Fe–P Systems. *Metals* **2024**, *14*, 1116. <https://doi.org/10.3390/met14101116>

Academic Editor: Andrii Kostryzhev

Received: 1 September 2024

Revised: 24 September 2024

Accepted: 26 September 2024

Published: 30 September 2024



Copyright: © 2024 by the authors. Licensee MDPI, Basel, Switzerland. This article is an open access article distributed under the terms and conditions of the Creative Commons Attribution (CC BY) license (<https://creativecommons.org/licenses/by/4.0/>).

1. Introduction

In recent years, the Cr–Fe–P system has attracted increasingly wide focus among researchers since it is vital for the metallurgical process of amorphous alloys, stainless steels, and semiconductors [1–5]. Such materials always exhibit excellent corrosion resistance, strength, thermal sensitivity, and photoconductive properties, which primarily depend on their chemical composition and preparation process. In order to fabricate Cr–Fe–P materials with promising performance, fundamental investigations of the thermodynamic behavior of the Cr–Fe–P alloy are of great significance as they help the alloy design and process optimization in actual practice.

Until now, the Cr–Fe [6–10] and Fe–P [11–17] systems have been thermodynamically modeled by many investigators and were reoptimized recently by the present authors [18,19]. A thermodynamic assessment of the Cr–P system was performed by Miettinen [20], who proposed only a partial Cr–P phase diagram of the Cr-rich region. The extrapolated phase diagram for the remaining region shows much discrepancy. Furthermore, the assessment results of the Cr–P system exhibited less satisfactory agreement with the thermodynamic property data of intermediate Cr phosphides and inconsistency with the ternary Cr–Fe–P system. A thermodynamic assessment of the ternary Cr–Fe–P system was performed by Miettinen and Vassilev [21]. However, the assessed model parameters result in some deviations of phase equilibria and thermodynamic properties from

existing data. Therefore, reoptimization of the Cr–Fe–P system is necessary to obtain a self-consistent and accurate thermodynamic description of this system.

The purpose of the present study is to conduct a critical thermodynamic optimization of the Cr–P and Cr–Fe–P systems to construct a more accurate thermodynamic database. The recently optimized Cr–Fe [18] and Fe–P [19] systems by the present authors were adopted by this work. The phase relation and thermodynamic properties of the Cr–P and Cr–Fe–P systems were optimized based on reliable experimental information. Particularly, the Gibbs energies of the liquid, CrP(s), CrP₂(s), (Cr,Fe)₃(P)₁, (Cr,Fe)₂(P)₁, (Cr,Fe)₁(P)₁, BCC_A2, and FCC_A1 phases were carefully determined to resolve the discrepancies left over in existing thermodynamic assessments [20,21]. The present Cr–Fe–P database was utilized to predict experimentally unexplored thermodynamic properties and phase diagrams. All the calculations were conducted using the FactSage 8.3 software [22].

2. Thermodynamic Models

2.1. Gas Phase

The gas phase of the Cr–Fe–P system is a mixture of Cr(g), Fe(g), P(g), P₂(g), and P₄(g) species. The molar Gibbs energy of gas phase (G_T^{gas}) was determined by Equation (1):

$$G_T^{\text{gas}} = \sum x_i \left(G_i^\circ + RT \ln x_i \right) + RT \ln \left(f / P^\theta \right) \quad (1)$$

where G_i° is the molar Gibbs energy (J/mol) of gas species i and was taken directly from the FactPS database of FactSage [22], R is the molar gas constant ($=8.314 \text{ J}/(\text{mol} \cdot \text{K})$), x_i is the mole fraction of gas species i , f is the gas fugacity and identical to the gas pressure (in atm) at normal pressure, T is the temperature in Kelvin (K), P^θ is the atmospheric pressure ($=1 \text{ atm}$), and f is the gas fugacity that is identical to the gas pressure (in atm) at normal pressure.

2.2. Elementary Substance and Stoichiometric Compounds

The Gibbs energies of pure solid and liquid Cr, Fe, and P elements were taken from the SGTE [23] data compilation. No stoichiometric compound was considered for the binary Cr–Fe and ternary Cr–Fe–P systems. The Gibbs energies (G_T°) of all intermediate compounds including Cr₃P, Cr₂P, CrP, and CrP₂ of the Cr–P system and Fe₃P, Fe₂P, FeP, and FeP₂ of the Fe–P system could be determined by their standard enthalpy of formation $\Delta H_{298.15 \text{ K}}^\circ$ (J/mol), heat capacity C_P (J/(mol·K)), and standard entropy $S_{298.15 \text{ K}}^\circ$ (J/(mol·K)), as expressed by Equation (2):

$$G_T^\circ = \left(\Delta H_{298.15 \text{ K}}^\circ + \int_{298.15 \text{ K}}^T C_P dT \right) - T \left(S_{298.15 \text{ K}}^\circ + \int_{298.15 \text{ K}}^T \frac{C_P}{T} dT \right) \quad (2)$$

In particular, an additional Gibbs energy resulting from the magnetic contribution, G^{mg} (J/mol), was applied to the Gibbs energies of Cr(BCC_A2, FCC_A1), Fe(BCC_A2, FCC_A1), and Fe₃P, which exhibits magnetic behavior, based on an empirical expression proposed by Inden [24] and modified by Hillert and Jarl [25]:

$$G^{\text{mg}} = RT \ln(\beta + 1) g(\tau) \quad (3)$$

where τ is expressed by T/T^* , T^* is the Néel temperature T_N (K) for anti-ferromagnetic ordering or the Curie temperature T_C (K) for ferromagnetic ordering, β is the average magnetic moment of per mole of atoms expressed in Bohr magnetons (μ_B/mol), and $g(\tau)$ is a polynomial function that can be determined by Equation (4) [25]:

$$\begin{aligned} g(\tau) &= 1 - \left[\frac{79\tau^{-1}}{140p} + \frac{474}{497} \left(\frac{1}{p} - 1 \right) \left(\frac{\tau^3}{6} + \frac{\tau^9}{135} + \frac{\tau^{15}}{600} \right) \right] / D, \dots \tau \leq 1 \\ g(\tau) &= - \left(\frac{\tau^{-5}}{10} + \frac{\tau^{-15}}{315} + \frac{\tau^{-25}}{1500} \right) / D, \dots \tau > 1 \end{aligned} \quad (4)$$

where $D = \frac{518}{1125} + \frac{11692}{15975} \left(\frac{1}{p} - 1 \right)$, and the p value was considered as the fraction of the magnetic enthalpy absorbed above the critical temperature depending on the structure; for example, p is 0.40 for BCC_A2 phase and 0.28 for other common phases.

2.3. Solid Solutions

The Gibbs energies of solid solutions of the Cr–Fe–P system were described using the Compound Energy Formalism (CEF) [26] with consideration of their crystal structures. In the ternary Cr–Fe–P system, isomorphous Cr_3P and Fe_3P ; Cr_2P and Fe_2P ; and CrP and FeP can form solid solutions in the formulas of Me_3P , Me_2P , and MeP , respectively, through mutual substitution between Cr and Fe atoms. In the present study, the solid Me_3P , Me_2P , and MeP solutions were described using a two-sublattice model $(\text{Cr,Fe})_n(\text{P})$ ($n = 3$ for Me_3P , $n = 2$ for Me_2P , and $n = 1$ for MeP). Their molar Gibbs energies can be calculated by Equation (5).

$$G_{\text{Me}_n\text{P}}^{\text{sol}} = y_{\text{Cr}} G_{\text{Cr}_n\text{P}}^{\circ} + y_{\text{Fe}} G_{\text{Fe}_n\text{P}}^{\circ} + nRT(y_{\text{Cr}} \ln y_{\text{Cr}} + y_{\text{Fe}} \ln y_{\text{Fe}}) + \sum_{i=0,1,2,\dots} y_{\text{Cr}} y_{\text{Fe}} L_{\text{Cr,Fe:P}}^i + G^{\text{mg}} \quad (5)$$

where, y_{Cr} and y_{Fe} are site fractions of Cr and Fe in the substitutional lattice. $G_{\text{Cr}_n\text{P}}^{\circ}$ and $G_{\text{Fe}_n\text{P}}^{\circ}$ are Gibbs energies (J/mol) of Cr_nP and Fe_nP compounds, respectively. $L_{\text{Cr,Fe:P}}^i$ is the adjustable interaction parameter. G^{mg} is the magnetic contribution to the Gibbs energy. BCC_A2 and FCC_A1 solid solutions were described using the model $(\text{Cr,Fe,P})_1(\text{Va})_j$ ($j = 1, 3$ for BCC_A2 and 1 for FCC_A1), and their Gibbs energies per formula unit were calculated as follows:

$$G_{\text{BCC/FCC}}^{\text{sol}} = \sum_{i=\text{Fe,Cr,P}} x_i G_i^{\circ} + RT \sum_{i=\text{Fe,Cr,P}} x_i \ln x_i + \sum_{m=0,1,2,\dots} x_{\text{Cr}} x_{\text{P}} L_{\text{Cr,P:Va}}^m + \sum_{k=0,1,2,\dots} x_{\text{Fe}} x_{\text{P}} L_{\text{Fe,P:Va}}^k + \sum_{p=0,1,2,\dots} x_{\text{Cr}} x_{\text{Fe}} L_{\text{Cr,Fe:Va}}^p + \sum_{q=0,1,2,\dots} x_{\text{Fe}} x_{\text{Cr}} x_{\text{P}} L_{\text{Fe,Cr,P:Va}}^q + G^{\text{mg}} \quad (6)$$

where x_i is the mole fraction of component i ; G_i° is the molar Gibbs energy (J/mol) of pure solid i ($i = \text{Cr, Fe, P}$); and $L_{\text{Cr,P}}^m$, $L_{\text{Fe,P}}^k$, $L_{\text{Fe,P}}^p$ and $L_{\text{Fe,Cr,P}}^q$ are adjustable interaction parameters of corresponding binary and ternary systems (J/mol). The sigma phase was described with a three-sublattice model $(\text{Fe})_8(\text{Cr})_4(\text{Fe,Cr})_{18}$, and its molar Gibbs energy was calculated using Equation (7):

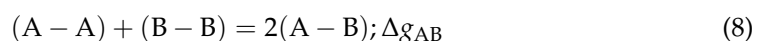
$$G_{\text{Sigma}}^{\text{sol}} = y_{\text{Fe}} G_{\text{Fe}_8\text{Cr}_4\text{Fe}_{18}}^{\circ} + y_{\text{Cr}} G_{\text{Fe}_8\text{Cr}_4\text{Cr}_{18}}^{\circ} + 18RT(y_{\text{Fe}} \ln y_{\text{Fe}} + y_{\text{Cr}} \ln y_{\text{Cr}}) + \sum_{i=0,1,2,\dots} y_{\text{Fe}} y_{\text{Cr}} L_{\text{Fe:Cr:Fe,Cr}}^i \quad (7)$$

where $G_{\text{Fe}_8\text{Cr}_4\text{Fe}_{18}}^{\circ}$ and $G_{\text{Fe}_8\text{Cr}_4\text{Cr}_{18}}^{\circ}$ are the Gibbs energies (J/mol) of $\text{Fe}_8\text{Cr}_4\text{Fe}_{18}$ and $\text{Fe}_8\text{Cr}_4\text{Cr}_{18}$ combinations, respectively. $L_{\text{Fe:Cr:Fe,Cr}}^i$ is the adjustable interaction model parameter (J/mol).

2.4. Liquid Solution

The modified quasichemical model (MQM) [27,28], accounting for the short-range ordering (SRO) of the nearest-neighbor atoms, was utilized to describe the liquid phases of all subsystems and the entire ternary system of Cr–Fe–P. Compared to the traditional Bragg–Williams random mixing model, the MQM gives a more realistic thermodynamic description of the liquid solution. In MQM, the atom pair formation Gibbs energy can be expressed as a polynomial of the pair fraction instead of the component fraction, and the coordination number of each component can be varied with composition to reproduce the SRO more easily.

For the binary A–B liquid solution, A and B atoms are distributed over the quasilattice sites, and the following atom pair exchanging reaction is considered in MQM:



where (A–A), (A–B), and (B–B) represent the first-nearest-neighbor pairs between components A and A, A and B, and B and B; and Δg_{AB} is the formation Gibbs energy of 2 moles

of (A–B) pairs from 1 mole (A–A) pairs and 1 mole (B–B) pairs. The Gibbs energy of the A–B liquid phase was calculated as follows:

$$G_{AB}^{\text{Liq.}} = (n_A G_A^\circ + n_B G_B^\circ) - T \Delta S_{AB}^{\text{conf.}} + n_{AB} (\Delta g_{AB} / 2) \quad (9)$$

where n_A and n_B are the mole numbers of A and B atoms (mol), G_A° and G_B° are molar Gibbs energies of pure liquid A and B (J/mol), and $\Delta S_{AB}^{\text{conf.}}$ is the configurational entropy of mixing (J/(mol·K)) given by random distribution of the (A–A), (A–B), and (B–B) pairs as follows:

$$\Delta S_{AB}^{\text{conf.}} = -R(n_A \ln X_A + n_B \ln X_B) - R \left[n_{AA} \ln \left(\frac{X_{AA}}{Y_A^2} \right) + n_{BB} \ln \left(\frac{X_{BB}}{Y_B^2} \right) + n_{AB} \ln \left(\frac{X_{AB}}{2Y_A Y_B} \right) \right] \quad (10)$$

where n_{AA} , n_{AB} , and n_{BB} represent the mole numbers of (A–A), (A–B), and (B–B) pairs (mol); X_{AA} , X_{AB} , and X_{BB} are pair fractions of corresponding atom pairs; and Y_A and Y_B are coordination equivalent fractions of A and B atoms. The pair fractions X_{AA} , X_{BB} , and X_{AB} and coordination equivalent fractions Y_A and Y_B were determined by Equations (11)–(15):

$$X_{AA} = n_{AA} / (n_{AA} + n_{AB} + n_{BB}) \quad (11)$$

$$X_{AB} = n_{AB} / (n_{AA} + n_{AB} + n_{BB}) \quad (12)$$

$$X_{BB} = n_{BB} / (n_{AA} + n_{AB} + n_{BB}) \quad (13)$$

$$Y_A = X_{AA} + \frac{1}{2} X_{AB} \quad (14)$$

$$Y_B = X_{BB} + \frac{1}{2} X_{AB} \quad (15)$$

Δg_{AB} in Equations (8) and (9) is the model parameter to reproduce the Gibbs energy of the A–B liquid solution (J/mol), and can be expanded as a polynomial in terms of the atomic pair fractions X_{AA} and X_{BB} .

$$\Delta g_{AB} = \Delta g_{AB}^\circ + \sum_{i \geq 1} g_{AB}^{i0} X_{AA}^i + \sum_{j \geq 1} g_{AB}^{0j} X_{BB}^j \quad (16)$$

where Δg_{AB}° , g_{AB}^{i0} , and g_{AB}^{0j} are adjustable model parameters (J/mol) that can be functions of the temperature. In MQM, the coordination numbers of A and B, and Z_A and Z_B , can be varied with the composition to reproduce the SRO as follows:

$$\frac{1}{Z_A} = \frac{1}{Z_{AA}^A} \left(\frac{2n_{AA}}{2n_{AA} + n_{AB}} \right) + \frac{1}{Z_{AB}^A} \left(\frac{n_{AB}}{2n_{AA} + n_{AB}} \right) \quad (17)$$

$$\frac{1}{Z_B} = \frac{1}{Z_{BB}^B} \left(\frac{2n_{BB}}{2n_{BB} + n_{AB}} \right) + \frac{1}{Z_{BA}^B} \left(\frac{n_{AB}}{2n_{BB} + n_{AB}} \right) \quad (18)$$

where Z_{AA}^A is the value Z_A when all nearest neighbors of an A atom are A atoms, and Z_{AB}^A is the value of Z_A when all nearest neighbors of the A atom are B atoms. Z_{BB}^B and Z_{BA}^B are defined in an analogous manner. In this study, $Z_{CrCr}^{\text{Cr}} = Z_{FeFe}^{\text{Fe}} = Z_{PP}^{\text{P}} = 6$ [18,19], $Z_{PFe}^{\text{P}} = Z_{PCr}^{\text{P}} = Z_{FeCr}^{\text{Fe}} = Z_{CrFe}^{\text{Cr}} = 6$ [18,19], and $Z_{FeP}^{\text{Fe}} = Z_{CrP}^{\text{Cr}} = 3$ [19], as given in Table 1.

Table 1. Optimized model parameters of the Cr–Fe–P system. Heat capacity, C_P (J/(mol·K)); standard enthalpy of formation, $\Delta H_{298.15\text{ K}}^\circ$ (J/mol); standard entropy, $S_{298.15\text{ K}}^\circ$ (J/(mol·K)); adjustable interaction parameter, L (J/mol); Gibbs energy, G , g , Δg (J/mol); Curie temperature, T_C (K); magnetic moment, β (μ_B /mol).

Phase	Model Parameters
Liquid (Cr, Fe, P)	$Z_{\text{CrCr}}^{\text{Cr}} = Z_{\text{FeFe}}^{\text{Fe}} = Z_{\text{PP}}^{\text{P}} = 6$ [18,19] $Z_{\text{PCr}}^{\text{P}} = Z_{\text{PFe}}^{\text{P}} = Z_{\text{CrFe}}^{\text{Cr}} = Z_{\text{FeCr}}^{\text{Fe}} = 6$ [18,19] $Z_{\text{CrP}}^{\text{Cr}} = Z_{\text{FeP}}^{\text{Fe}} = 3$ [19] $\Delta g_{\text{CrP}} = -49,078 - 3.5564T + (21,548 + 2.092T)X_{\text{CrCr}} - 29,957X_{\text{CrCr}}^2$ [*] $\Delta g_{\text{FeP}} = -56,902 + 6.569T + (5481 + 3.033T)X_{\text{FeFe}} - (11,966 - 2.51T)X_{\text{FeFe}}^2 - 9623X_{\text{PP}}$ [19] $\Delta g_{\text{CrFe}} = -242 - 0.335T - (192.46 + 1.046T)X_{\text{CrCr}} + 83.68X_{\text{FeFe}}$ [18] $g_{\text{CrP(Fe)}}^{001} = 8368$ [*], $g_{\text{FeP(Cr)}}^{001} = -37,237.6 + 7.5312T$ [*], $g_{\text{FeCr(P)}}^{001} = 4184 + 12.552T$ [*] “Toop-like” interpolation with P as an asymmetric component [*]
BCC_A2 (Cr,Fe,P) ₁ (Va) ₃	$G_{\text{Fe:Va}}^{\text{BCC_A2}} = G_{\text{Fe(BCC)}}^\circ$, $G_{\text{Cr:Va}}^{\text{BCC_A2}} = G_{\text{Cr(BCC)}}^\circ$, $G_{\text{P:Va}}^{\text{BCC_A2}} = G_{\text{P(BCC)}}^\circ$ [*] $L_{\text{Cr,P:Va}}^{\text{BCC_A2}} = -48,116$ [*] $L_{\text{Fe,P:Va}}^{\text{BCC_A2}} = -203,476 + 15.48T + 33,472(y_{\text{Fe}} - y_{\text{P}})$ [19] $L_{\text{Fe,Cr:Va}}^{\text{BCC_A2}} = 20,502 - 9.68T$ [9] $T_{\text{CCr:Va}} = -311$ [21], $T_{\text{CFe:Va}} = 1043$ [29] $T_{\text{CFe,P:Va}} = -285$ [19], $T_{\text{CFe,Cr:Va}} = 1650 - 550(x_{\text{Fe}} - x_{\text{Cr}})$ [9] $\beta_{\text{Fe:Va}} = 2.22$ [29], $\beta_{\text{Cr:Va}} = -0.008$ [6], $\beta_{\text{Fe,Cr:Va}} = -0.85$ [6]
FCC_A1 (Cr,Fe,P) ₁ (Va) ₁	$G_{\text{Fe:Va}}^{\text{FCC}} = G_{\text{Fe(FCC)}}^\circ$, $G_{\text{Cr:Va}}^{\text{FCC}} = G_{\text{Cr(FCC)}}^\circ$, $G_{\text{P:Va}}^{\text{FCC}} = G_{\text{P(FCC)}}^\circ$ [*] $L_{\text{Cr,P:Va}}^{\text{FCC_A1}} = L_{\text{Cr,P:Va}}^{\text{BCC_A2}} = -48,116$ [*] $L_{\text{Fe,P:Va}}^{\text{FCC}} = -139,787 + 6.49T$ [19] $L_{\text{Fe,Cr:Va}}^{\text{FCC_A1}} = 10,833 - 7.477T - 1410(x_{\text{Fe}} - x_{\text{Cr}})$ [6] $T_{\text{CCr:Va}} = -1109$, $T_{\text{CFe:Va}} = -201$ [6] $\beta_{\text{Cr:Va}} = -2.46$ [6], $\beta_{\text{Fe:Va}} = -2.1$ [29]
Sigma (Fe) ₈ (Cr) ₄ (Fe,Cr) ₁₈	$G_{\text{Fe8Cr4Fe18}} = 8G_{\text{Fe(FCC_A1)}}^\circ + 4G_{\text{Cr(BCC_A2)}}^\circ + 18G_{\text{Fe(BCC_A2)}}^\circ + 117,300 - 95.96T$ [6] $G_{\text{Fe8Cr4Cr18}} = 8G_{\text{Fe(FCC_A1)}}^\circ + 22G_{\text{Cr(BCC_A2)}}^\circ + 92,300 - 95.96T$ [6]
Me ₃ P (Cr,Fe) ₃ (P) ₁	$G_{\text{Fe:P}}^{\text{Me}_3\text{P}} = G_{\text{Fe}_3\text{P}}^\circ$ [19] $G_{\text{Cr:P}}^{\text{Me}_3\text{P}} = G_{\text{Cr}_3\text{P}}^\circ$ [*] $\Delta H_{298.15\text{ K}}^\circ(\text{Cr}_3\text{P}) = -184,880$, $S_{298.15\text{ K}}^\circ(\text{Cr}_3\text{P}) = 93.3$ [*] $C_P(\text{Cr}_3\text{P}) = 99.258 + 0.0075T - 760,000T^{-2} + 1.9 \times 10^{-5}T^2$ [*] $L_{\text{Cr,Fe:P}}^{\text{Me}_3\text{P}} = -52,718 + 20.92T - 18,828(x_{\text{Cr}} - x_{\text{Fe}})$ [*]
Me ₂ P (Cr,Fe) ₂ (P) ₁	$G_{\text{Fe:P}}^{\text{Me}_2\text{P}} = G_{\text{Fe}_2\text{P}}^\circ$ [19] $G_{\text{Cr:P}}^{\text{Me}_2\text{P}} = G_{\text{Cr}_2\text{P}}^\circ$ [*] $\Delta H_{298.15\text{ K}}^\circ(\text{Cr}_2\text{P}) = -169,890$, $S_{298.15\text{ K}}^\circ(\text{Cr}_2\text{P}) = 74$ [*] $C_P(\text{Cr}_2\text{P}) = 76.85 + 0.0058T - 476,000T^{-2} + 9.8 \times 10^{-6}T^2$ [*] $L_{\text{Cr,Fe:P}}^{\text{Me}_2\text{P}} = -45,187 + 5.4392T$ [*]
MeP (Cr,Fe) ₁ (P) ₁	$G_{\text{Fe:P}}^{\text{MeP}} = G_{\text{FeP}}^\circ$ [19] $G_{\text{Cr:P}}^{\text{MeP}} = G_{\text{CrP}}^\circ$ [*] $\Delta H_{298.15\text{ K}}^\circ(\text{CrP}) = -122,700$, $S_{298.15\text{ K}}^\circ(\text{CrP}) = 46.4$ [*] $C_P(\text{CrP}) = 47.692 + 0.01233305T - 200,250T^{-2} + 1.1051 \times 10^{-6}T^2$ [*] $L_{\text{Cr,Fe:P}}^{\text{MeP}} = -20,083$ [*]
CrP ₂ (Cr) ₁ (P) ₂	$\Delta H_{298.15\text{ K}}^\circ(\text{CrP}_2) = -155,895$, $S_{298.15\text{ K}}^\circ(\text{CrP}_2) = 63$ [*] $C_P = 68.476 + 0.0284548T - 122,000T^{-2} - 6.253 \times 10^{-6}T^2$ [*]
FeP ₂ (Fe) ₁ (P) ₂	$\Delta H_{298.15\text{ K}}^\circ = -191,100$, $S_{298.15\text{ K}}^\circ = 51.05$ [19] $C_P = 77.52563 + 0.009348T - 443,846T^{-2} - 1.1 \times 10^{-6}T^2$ [19]

* optimized in the present study.

The Gibbs energy of the ternary Cr–Fe–P liquid phase can be calculated by interpolating the Gibbs energies of its binary subsystems. In MQM, different geometric interpolation

techniques [28] can be utilized depending on the nature of the involved binary liquid solutions to improve the predictive capability. In this work, an asymmetric “Toop-like” geometric interpolation with P as the “asymmetric component” was selected for the ternary Cr–Fe–P system, since the Cr–P and Fe–P liquid solutions deviate largely from the ideal mixing while the Cr–Fe liquid solution exhibits in almost ideal mixing. Based on this interpolation, the Gibbs energy and entropy of mixing of the ternary Cr–Fe–P liquid solution can be calculated by Equations (19) and (20):

$$G_{\text{CrFeP}}^{\text{Liq.}} = \sum_{i=\text{Cr,Fe,P}} n_i G_i^{\circ} - T \Delta S_{\text{CrFeP}}^{\text{conf.}} + \sum_{j,k=\text{Cr,Fe,P}}^{j \neq k} \left(n_{jk}/2 \right) \Delta g_{jk} \quad (19)$$

$$\Delta S_{\text{CrFeP}}^{\text{conf.}} = -R \sum_{i=\text{Cr,Fe,P}} n_i \ln X_i - R \left[\sum_{j=\text{Cr,Fe,P}} n_{jj} \left(\frac{X_{jj}}{Y_j^2} \right) + \sum_{k,m=\text{Cr,Fe,P}}^{k \neq m} n_{km} \ln \left(\frac{X_{km}}{2Y_k Y_m} \right) \right] \quad (20)$$

where Δg_{jk} ($j, k = \text{Cr, Fe, P}$) is the pair formation Gibbs energy depending on the thermodynamic symmetry of the ternary system. Δg_{CrP} and Δg_{FeP} for the asymmetric Cr–P and Fe–P systems were calculated using Equations (21) and (22), respectively:

$$\Delta g_{\text{CrP}} = \Delta g_{\text{CrP}}^{\circ} + \sum_{(i+j) \geq 1} g_{\text{CrP}}^{ij} x_{\text{PP}}^i (x_{\text{CrCr}} + x_{\text{CrFe}} + x_{\text{FeFe}})^j + \sum_{i \geq 0, j \geq 0, k \geq 1} g_{\text{CrP(Fe)}}^{ijk} x_{\text{PP}}^i (x_{\text{CrCr}} + x_{\text{CrFe}} + x_{\text{FeFe}})^j \left(\frac{Y_{\text{Fe}}}{Y_{\text{Cr}} + Y_{\text{Fe}}} \right)^k \quad (21)$$

$$\Delta g_{\text{FeP}} = \Delta g_{\text{FeP}}^{\circ} + \sum_{(i+j) \geq 1} g_{\text{FeP}}^{ij} x_{\text{PP}}^i (x_{\text{CrCr}} + x_{\text{CrFe}} + x_{\text{FeFe}})^j + \sum_{i \geq 0, j \geq 0, k \geq 1} g_{\text{FeP(Cr)}}^{ijk} x_{\text{PP}}^i (x_{\text{CrCr}} + x_{\text{CrFe}} + x_{\text{FeFe}})^j \left(\frac{Y_{\text{Cr}}}{Y_{\text{Cr}} + Y_{\text{Fe}}} \right)^k \quad (22)$$

while Δg_{CrFe} for the symmetric Cr–Fe system was calculated by Equation (23):

$$\begin{aligned} \Delta g_{\text{CrFe}} = & \Delta g_{\text{CrFe}}^{\circ} + \sum_{(i+j) \geq 1} g_{\text{CrFe}}^{ij} \left(\frac{x_{\text{CrCr}}}{x_{\text{CrCr}} + x_{\text{CrFe}} + x_{\text{FeFe}}} \right)^i \left(\frac{x_{\text{FeFe}}}{x_{\text{CrCr}} + x_{\text{CrFe}} + x_{\text{FeFe}}} \right)^j \\ & + \sum_{i \geq 0, j \geq 0, k \geq 1} g_{\text{CrFe(P)}}^{ijk} \left(\frac{x_{\text{CrCr}}}{x_{\text{CrCr}} + x_{\text{CrFe}} + x_{\text{FeFe}}} \right)^i \left(\frac{x_{\text{FeFe}}}{x_{\text{CrCr}} + x_{\text{CrFe}} + x_{\text{FeFe}}} \right)^j Y_{\text{P}}^k \end{aligned} \quad (23)$$

where g_{CrP}^{ij} , g_{FeP}^{ij} , and g_{CrFe}^{ij} are binary model parameters (J/mol) and $g_{\text{CrP(Fe)}}^{ijk}$, $g_{\text{FeP(Cr)}}^{ijk}$, and $g_{\text{CrFe(P)}}^{ijk}$ are ternary model parameters (J/mol) of the liquid solution.

3. Critical Evaluation and Thermodynamic Optimization

Thermodynamic optimization of the binary Cr–P and ternary Cr–Fe–P systems was conducted based on critical evaluation of all the experimental thermodynamic property and phase diagram data. The optimized model parameters of the whole Cr–Fe–P system are summarized in Table 1. The details of the present thermodynamic modeling are given in the following sections.

3.1. The Cr–P System

The experimental information of the partial phase diagram and various intermediate Cr phosphides, including $\text{Cr}_3\text{P(s)}$ [30–37], $\text{Cr}_2\text{P(s)}$ [32,33,38–41], $\text{Cr}_{12}\text{P}_7\text{(s)}$ ($\text{Cr}_{1.7}\text{P(s)}$) [38–40,42–45], CrP(s) [31,33,34,46–56], $\text{Cr}_2\text{P}_3\text{(s)}$ [49], $\text{CrP}_2\text{(s)}$ [33,34,57], and $\text{CrP}_4\text{(s)}$ [58,59], of the Cr–P system were reviewed by Venkatraman and Neumann [60]. $\text{Cr}_3\text{P(s)}$, CrP(s) , and $\text{CrP}_2\text{(s)}$ are commonly confirmed as stable compounds of the Cr–P system. However, the existence of $\text{Cr}_2\text{P}_3\text{(s)}$ was refuted by subsequent study [33] and the evidence for the presence of $\text{CrP}_4\text{(s)}$ is insufficient. According to the literature [38,40], the stoichiometry of the compound between $\text{Cr}_3\text{P(s)}$ and CrP(s) is ambiguous. So far, two primary phosphides, $\text{Cr}_{12}\text{P}_7\text{(s)}$ and $\text{Cr}_2\text{P(s)}$, have been proposed as intermediate compounds by various investigators [32,33,38–45]. Nevertheless, their thermodynamic stability is controversial in the literature. After careful examination, it was found that isomorphous $\text{Fe}_2\text{P(s)}$ and $\text{Cr}_2\text{P(s)}$ exhibit mutual solubility in each other to form a homogeneous ternary $(\text{Cr,Fe})_2\text{P}$

solid solution [31,32,61], and $\text{Cr}_{12}\text{P}_7(\text{s})$ has been reported to occur in a small homogeneity range [38]. Hence, $\text{Cr}_{12}\text{P}_7(\text{s})$ is more likely to be a metastable phase of the Cr–P system. It is well known that solid Cr and P show negligible solubility in each other. In the present study, stoichiometric $\text{Cr}_3\text{P}(\text{s})$, $\text{Cr}_2\text{P}(\text{s})$, $\text{CrP}(\text{s})$, and $\text{CrP}_2(\text{s})$ compounds, liquid and gas phases, are thus considered as stable phases of the Cr–P system.

3.1.1. The Cr–P Phase Diagram

The calculated Cr–P phase diagram calculated from the previous assessment and the present study are compared with the experimental data [32,62] in Figure 1. The early experimental data for the liquidus and solidus of the Cr–P system were reported by Vogel and Kasten [32] based on the thermal analysis and metallographic analysis. They suggested a eutectic reaction $\text{liquid}(x_{\text{P}} = 0.134) = \text{Cr} + \text{Cr}_3\text{P}(\text{s})$ at around 1376 °C. The other set of data by Zaitsev et al. [62] were integrated from the thermodynamic properties of Cr–P melts and Cr phosphides based on the Knudsen effusion experiments. Compared to the former experimental data, the data of Zaitsev et al. [62] are shifted towards the P-richer region and were less favored by both thermodynamic modelings. In the modeling of Miettinen [20], only a partial phase diagram of $x_{\text{P}} = 0 \sim 0.36$ was assessed with consideration of the liquid solution and two intermediate compounds ($\text{Cr}_3\text{P}(\text{s})$, $\text{Cr}_2\text{P}(\text{s})$). The extrapolated diagram for $x_{\text{P}} = 0.36 \sim 1$ from Miettinen’s parameters shows a “concave shape” of liquidus lines, which are even below the “freezing temperature” in the range of $x_{\text{P}} = 0.69 \sim 0.86$, as shown in the figure. In the present study, the P-rich phase diagram was modified by introducing another two compounds, $\text{CrP}(\text{s})$ and $\text{CrP}_2(\text{s})$, which have been reported by many researchers [31,33,34,46–57]. The optimized invariant reactions of the Cr–P system from the present study are compared with those from the previous assessment and experimental data in Table 2.

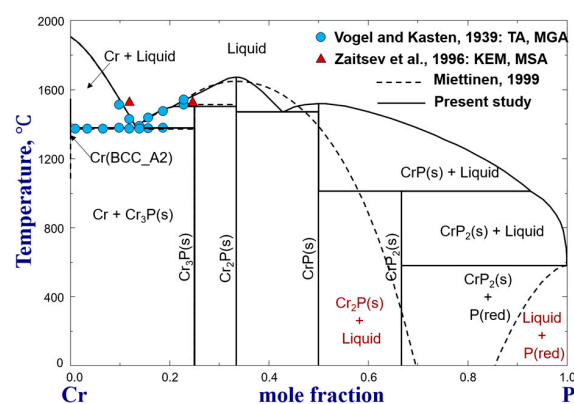


Figure 1. Calculated phase diagrams of the Cr–P system, compared to the experimental data [32,62].

Table 2. Invariant reactions involved in the Cr–P system.

Type	Reactions	Temperature, °C	References
Eutectic	$\text{Liquid}(x_{\text{P}} = 0.134) \rightarrow \text{Cr}(x_{\text{P}} = 0) + \text{Cr}_3\text{P}(x_{\text{P}} = 0.25)$	1371	[32]
	$\text{Liquid}(x_{\text{P}} = 0.134) \rightarrow \text{Cr}(x_{\text{P}} = 9.6 \times 10^{-5}) + \text{Cr}_3\text{P}(x_{\text{P}} = 0.25)$	1376	[20]
	$\text{Liquid}(x_{\text{P}} = 0.134) \rightarrow \text{Cr}(x_{\text{P}} = 2.7 \times 10^{-5}) + \text{Cr}_3\text{P}(x_{\text{P}} = 0.25)$	1376	Present study
Incongruent	$\text{Liquid}(x_{\text{P}} = 0.220) + \text{Cr}_2\text{P}(x_{\text{P}} = 0.333) \rightarrow \text{Cr}_3\text{P}(x_{\text{P}} = 0.25)$	1511	[20]
	$\text{Liquid}(x_{\text{P}} = 0.208) + \text{Cr}_2\text{P}(x_{\text{P}} = 0.333) \rightarrow \text{Cr}_3\text{P}(x_{\text{P}} = 0.25)$	1501	Present study
Congruent	$\text{Liquid}(x_{\text{P}} = 0.333) \rightarrow \text{Cr}_2\text{P}(x_{\text{P}} = 0.333)$	1642	[20]
	$\text{Liquid}(x_{\text{P}} = 0.333) \rightarrow \text{Cr}_2\text{P}(x_{\text{P}} = 0.333)$	1671	Present study
Eutectic	$\text{Liquid}(x_{\text{P}} = 0.428) \rightarrow \text{Cr}_2\text{P}(x_{\text{P}} = 0.333) + \text{CrP}(x_{\text{P}} = 0.5)$	1469	Present study
Congruent	$\text{Liquid}(x_{\text{P}} = 0.5) \rightarrow \text{CrP}(x_{\text{P}} = 0.5)$	1518	Present study
Incongruent	$\text{Liquid}(x_{\text{P}} = 0.926) + \text{CrP}(x_{\text{P}} = 0.5) \rightarrow \text{CrP}_2(x_{\text{P}} = 0.667)$	1011	Present study
Eutectic	$\text{Liquid}(x_{\text{P}} = 0.9995) \rightarrow \text{CrP}_2(x_{\text{P}} = 0.667) + \text{P}(x_{\text{P}} = 1.0)$	579	Present study

3.1.2. Thermodynamic Stability of Cr Phosphides

The thermodynamic stability of Cr phosphides has been widely investigated by many researchers [33,44,45,63–68]. Thermodynamic property data including the heat capacity (C_p) [45], standard enthalpy of formation ($\Delta H_{298.15\text{ K}}^\circ$) [44,45,63–65], standard entropy ($S_{298.15\text{ K}}^\circ$) [44,45,63–66], formation Gibbs energy (ΔG_f°) [44,45,67,68], and partial pressure of $P_2(g)$ or $P_4(g)$ over various Cr phosphides [33,44,45,68] were collected for critical optimization of their Gibb energies.

The C_p data of $Cr_3P(s)$ and $Cr_{12}P_7(s)$ were measured by Zaitsev et al. [45] using the differential scanning calorimetry method. As was discussed above, $Cr_{12}P_7(s)$ should be a metastable intermediate phase of forming $Cr_2P(s)$. Thus, the reported C_p values of $Cr_{12}P_7(s)$ were converted to those of $Cr_2P(s)$ in the present thermodynamic modeling. Figure 2 shows the calculated C_p curves of $Cr_3P(s)$ and $Cr_2P(s)$ from the previous assessment [20] and the present study compared with the experimental data [45]. However, the assessed C_p values by Miettinen [20] deviate somewhat from the experimental data. These discrepancies were resolved based on the present optimization, as shown in Figure 2a,b. The C_p of $CrP(s)$ and $CrP_2(s)$, with no available experimental data in the literature, were determined based on those of $Cr_3P(s)$ and $Cr_2P(s)$: $C_p(CrP) = 0.5\{C_p(Cr_3P) + C_p(Cr_2P) - 3C_p(Cr, BCC_A2)\}$, $C_p(CrP_2) = C_p(Cr_3P) + C_p(Cr_2P) - 4C_p(Cr, BCC_A2)$. The determined $C_p(CrP)$ and $C_p(CrP_2)$ functions depending on the temperature are given in Table 1.

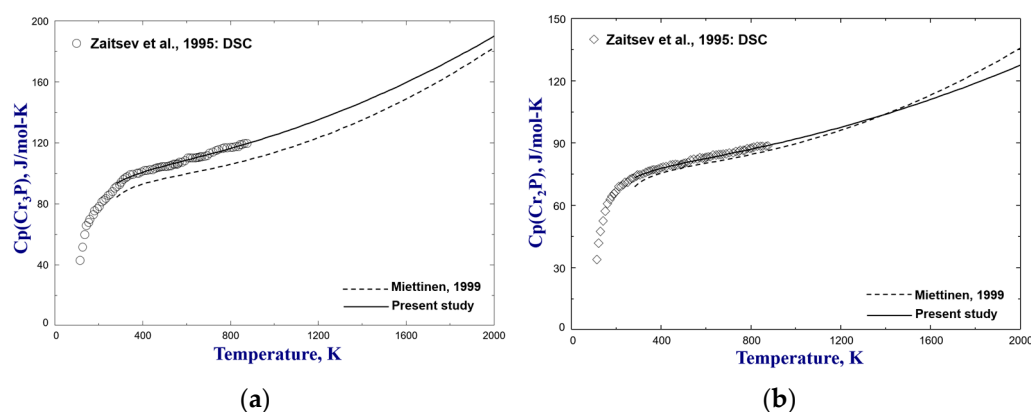


Figure 2. Calculated heat capacity of stoichiometric (a) Cr_3P and (b) Cr_2P compounds, compared to the experimental data [45].

The equilibrium $P_2(g)$ partial pressure over various Cr–P alloys was measured by Myers et al. [44] using the mass-loss effusion method at 1194 K to 1768 K and Zaitsev et al. [45] using the Knudsen effusion method at 1341 K to 1704 K. The obtained high-temperature vapor pressure data were used to determine the $\Delta H_{298.15\text{ K}}^\circ$ and $S_{298.15\text{ K}}^\circ$ values of involved Cr phosphides based on formulated C_p values. Glaum and Gruehn [63] determined the $\Delta H_{298.15\text{ K}}^\circ$ of $CrP(s)$ to be -124.15 ± 8.4 kJ/mol using the transportation method. The $\Delta H_{298.15\text{ K}}^\circ$ and $S_{298.15\text{ K}}^\circ$ for different Cr phosphides were also assessed/estimated by Schlesinger [64], Miettinen [20], Pogorelyi [65], and Kubaschewski and Alcock [66]. The experimental data and thermodynamic assessment/evaluation of $\Delta H_{298.15\text{ K}}^\circ$ and $S_{298.15\text{ K}}^\circ$ for $Cr_3P(s)$, $Cr_2P(s)$, $CrP(s)$, and $CrP_2(s)$ are listed in Table 3.

It is noticeable that the $\Delta H_{298.15\text{ K}}^\circ(Cr_3P) = -123.23$ kJ/mol by Myers et al. [44] is much less negative than the -184.26 ± 6.4 kJ/mol by Zaitsev et al., -180.51 kJ/mol by Schlesinger [64], and -177.58 kJ/mol by Miettinen [20]. Such big differences could be caused by non-negligible errors of high-temperature vapor pressure measurements or C_p estimation. In the present study, the $\Delta H_{298.15\text{ K}}^\circ$ for $Cr_3P(s)$ was optimized to be -184.88 kJ/mol by favoring the experimental data of Zaitsev et al. [45]. The $\Delta H_{298.15\text{ K}}^\circ$ for $Cr_2P(s)$ from thermodynamic assessment [20] is about 9.5 kJ/mol less negative than the only experimental value [45], which was determined to be -169.89 kJ/mol with slight

modification in the present study. The reported values of $\Delta H_{298.15\text{ K}}^\circ$ for CrP(s) show some fluctuation. In the present thermodynamic modeling, more weight was given to the experimental data of Glaum and Gruehn [63] (-124.15 ± 8.4 kJ/mol), as shown in Table 3. No experimental data are available in the literature for $\Delta H_{298.15\text{ K}}^\circ$ and $S_{298.15\text{ K}}^\circ$ of CrP₂(s). The only estimated $\Delta H_{298.15\text{ K}}^\circ$ value for CrP₂(s), -232.94 kJ/mol, was reported by Pogorelyi [65]. This value is apparently too negative and shows much inconsistency with the thermodynamic property data of other Cr phosphides. In the present study, the $\Delta H_{298.15\text{ K}}^\circ$ for CrP₂(s) was optimized to be -155.90 kJ/mol to reproduce the equilibrium pressure data of P₄(g) over CrP and CrP₂(s) [33].

Table 3. Standard enthalpy of formation (from BCC_A2 Cr and white P) and standard entropy (J/(mol·K)) of Cr phosphides.

Species	$\Delta H_{298.15\text{ K}}^\circ$, kJ/mol	$S_{298.15\text{ K}}^\circ$, J/(mol·K)	Techniques	References
Cr ₃ P	-184.26 ± 6.4	93.3	DSC	[45]
		94.3	KEM	
	-123.23 ± 1.3	87.9	MLE	[44]
	-180.51	93.1	Estimation	[64]
	-177.58	108.4	Assessment	[20]
	-184.88	93.3	Assessment	Present study
Cr ₂ P	-168.75 ± 5.4	74.0	DSC	[45]
		74.4	KEM	
	-159.28	83.2	Assessment	[20]
	-169.89	74.0	Assessment	Present study
CrP	-112.07 ± 3.0	39.7	MLE	[44]
	-124.15 ± 8.4		TM	[63]
	-138.06	46.9	Estimation	[64]
	-117.04	46.4	Estimation	[65]
		46.0	Estimation	[66]
	-122.70	46.4	Assessment	Present study
CrP ₂	-232.94		Estimation	[65]
	-155.90	63.0	Assessment	Present study

Based on the low-temperature C_p data and high-temperature vapor pressure data of Zaitsev et al. [45], $S_{298.15\text{ K}}^\circ$ was determined to be 93.3 J/(mol·K) and 94.3 J/(mol·K) for Cr₃P(s) and 74.0 J/(mol·K) and 74.4 J/(mol·K) for Cr₂P(s), respectively. As is well known, there is always potential error in the derivation of $S_{298.15\text{ K}}^\circ$ from high-temperature Gibbs energy data, while $S_{298.15\text{ K}}^\circ$ determined from low-temperature C_p data is more reliable. Therefore, the $S_{298.15\text{ K}}^\circ$ values measured by Myers et al. (87.9 J/(mol·K) for Cr₃P) [44] and assessed by Miettinen (108.4 J/(mol·K) for Cr₃P and 83.2 J/(mol·K) for Cr₂P) [20] are less reliable than those of Schlesinger (93.1 J/(mol·K) for Cr₃P) [64] and Zaitsev et al. (93.3 J/(mol·K) for Cr₃P and 74.0 J/(mol·K)) [45], which are adopted by the present study, as listed in Table 3. The $S_{298.15\text{ K}}^\circ$ values of CrP(s) suggested by Myers et al. (39.7 J/(mol·K)) [44] is inconsistent with those estimation values by Schlesinger (46.9 J/mol) [64], Pogorelyi (46.4 J/(mol·K)) [65], and Kubaschewski and Alcock (46.0 J/(mol·K)) [66]. According to the present modeling, it was found that $S_{298.15\text{ K}}^\circ = 46.4$ J/(mol·K) for CrP(s) could result in an overall accurate reproduction of the available phase diagram and thermodynamic property data of the Cr–P system. The $S_{298.15\text{ K}}^\circ$ for CrP₂(s) was determined to be 63.0 J/(mol·K) to reproduce the vapor pressure data [33].

Based on the optimized C_p , $\Delta H_{298.15\text{ K}}^\circ$, and $S_{298.15\text{ K}}^\circ$ of Cr₃P(s), Cr₂P(s), CrP(s), and CrP₂(s), the Gibbs energies of these compounds were determined from Equation (2).

Figure 3 shows the calculated formation Gibbs energies of Cr₃P(s) and Cr₂P(s) from the previous assessment [20] and the present study compared to the experimental data [44,45,67,68]. The experimental results of Zaitsev et al. [45] and Nagai et al. [67] are in reasonable agreement with each other but show much deviation from those of Myers et al. [44] and

Pogorelyi [68]. The former two sets of experimental data are favored by the present modeling, which shows certain improvements compared to the previous assessment. The calculated equilibrium partial pressure of $P_2(g)$ and $P_4(g)$ over $Cr_3P(s)$ and $Cr(s)$, $Cr_3P(s)$ and $Cr_2P(s)$, $Cr_2P(s)$ and $CrP(s)$, and $CrP(s)$ and $CrP_2(s)$ are presented in Figure 4 along with the experimental data [33,44,45,68]. Likewise, the experimental results of Myers et al. [44] and Pogorelyi [68] that are in poor consistency are not taken into account, while those of Zaitsev et al. [45] and Faller and Biltz [33] are well reproduced in this work, as shown in Figure 4. It is therefore expected that the optimized Gibbs energies of intermediate Cr phosphides should be accurate.

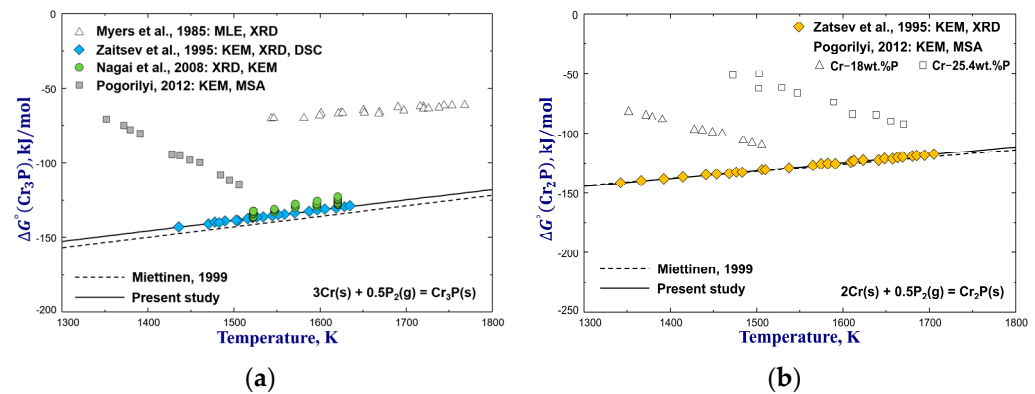


Figure 3. Calculated formation Gibbs energies of (a) Cr_3P and (b) Cr_2P from $Cr(BCC_A2)$ and $P_2(g)$, compared to the experimental data [44,45,67,68].

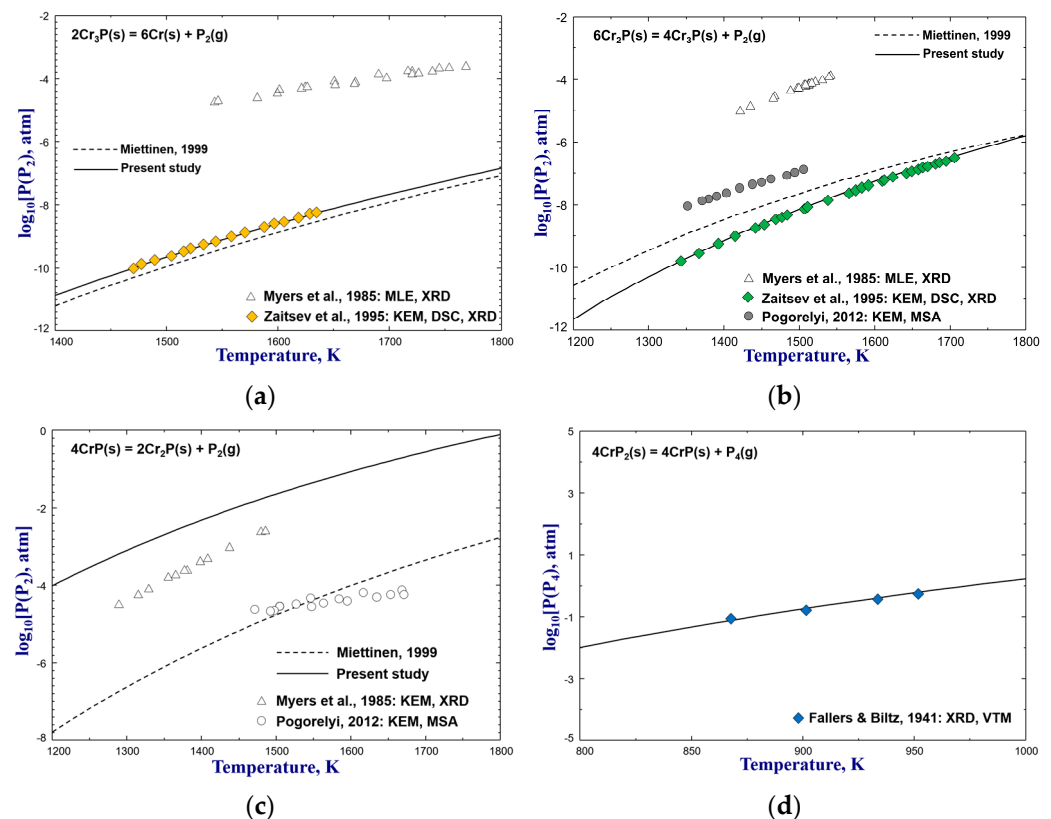


Figure 4. Calculated equilibrium partial pressure of $P_2(g)$ or $P_4(g)$ over (a) $Cr_3P(s)$ and $Cr(s)$, $2Cr_3P(s) = 6Cr(s) + P_2(g)$, (b) $Cr_3P(s)$ and $Cr_2P(s)$, $6Cr_2P(s) = 4Cr_3P(s) + P_2(g)$, (c) $Cr_2P(s)$ and $CrP(s)$, $4CrP(s) = 2Cr_2P(s) + P_2(g)$, and (d) $CrP(s)$ and $CrP_2(s)$, $4CrP_2(s) = 4CrP(s) + P_4(g)$, compared to the experimental data [33,44,45,68].

3.1.3. Thermodynamic Properties of the Cr–P Liquid Solution

The thermodynamic properties of the Cr–P liquid solution are of primary importance for process optimization of the Cr–P alloys. The activities of Cr(l) and P(l) in high-P Cr–P melts ($x_P = 0.08\sim 0.368$) at 1527 °C were also measured by Zaitsev et al. [62] using the mass spectrometry and Knudsen effusion techniques. The activity data were converted to corresponding partial chemical potentials and are presented in Figure 5 along with the previous and present modeling results. It is shown that the experimental data can be reproduced by both calculations within acceptable errors. So far, there is no available experimental information of the dilute Cr–P liquid solution due to the high melting point of Cr. According to the present optimization, the Henrian activity coefficient of P in Cr(l), $\gamma_{P \text{ in Cr(l)}}^\circ$, which is to quantify the deviation of P behavior from the ideal behavior particularly for the dilute region, was determined as a function of temperature as follows:

$$\ln \gamma_{P \text{ in Cr(l)}}^\circ = -\frac{20,742}{T} - 0.5285, \quad 2180 \text{ K} < T < 2573 \text{ K} \quad (24)$$

where T is the temperature in Kelvin (K). Based on the optimized $\gamma_{P \text{ in Cr(l)}}^\circ$, the molar Gibbs energies for the dissolution of P(g) and P₂(g) and into liquid Cr(1 wt.% standard state) were also determined, as expressed by Equations (25) and (26):

$$P(g) = [P]_{\text{in Cr(l)}}(1 \text{ wt. \%}), \Delta G_T^\circ = -477,073 + 70.4655(J/\text{mol}), \quad 2180 \text{ K} < T < 2573 \text{ K} \quad (25)$$

$$0.5P_2(g) = [P]_{\text{in Cr(l)}}(1 \text{ wt. \%}), \Delta G_T^\circ = -227,128 + 10.2395(J/\text{mol}), \quad 2180 \text{ K} < T < 2573 \text{ K} \quad (26)$$

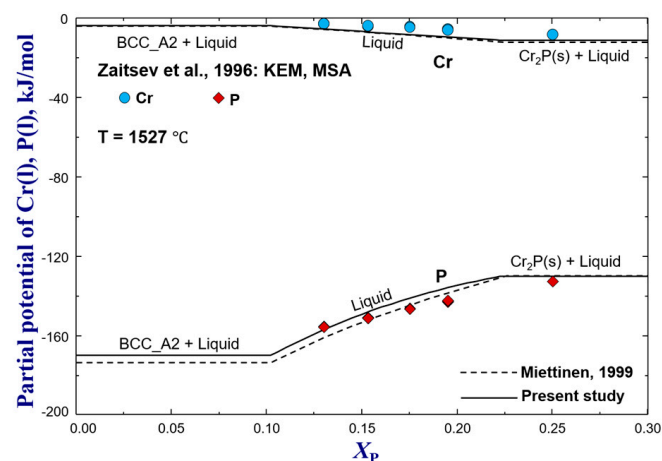


Figure 5. Calculated chemical potential of liquid Cr and P in Cr–P melts at 1527 °C (pure liquid Cr and P as reference states), compared to the experimental data [62].

3.2. The Cr–Fe and Fe–P Systems

Thermodynamic reoptimization of the Cr–Fe and Fe–P systems was performed recently by the present authors [18,19]. The optimized model parameters of these two systems were adopted by this study. Figure 6 shows the phase diagrams of the Fe–Cr and Fe–P systems. As shown in the figure, the gas, liquid solution, sigma, FCC_A1, BCC_A2, and BCC_A2#2 were taken as stable phases of the Cr–Fe system and the gas, liquid solution, FCC_A1, BCC_A2, Fe₃P(s), Fe₂P(s), FeP(s), and FeP₂(s) as stable phases of the Fe–P system.

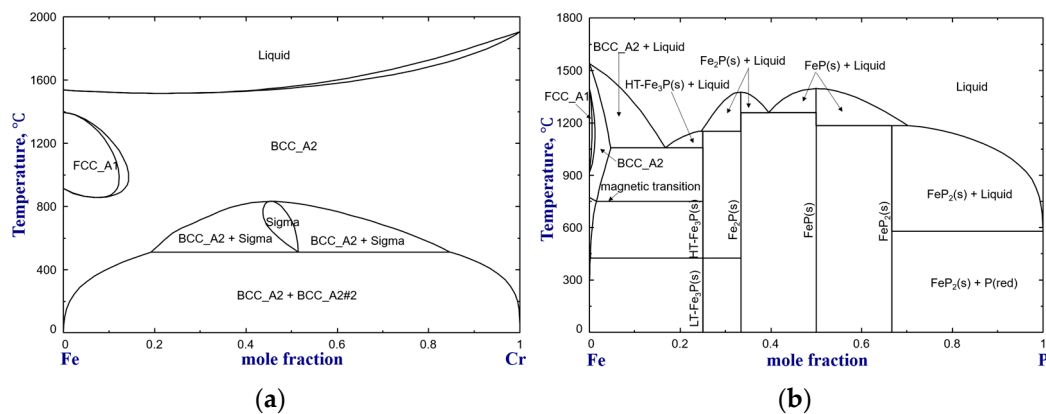


Figure 6. Phase diagrams of the (a) Fe–Cr and (b) Fe–P systems.

3.3. The Cr–Fe–P Systems

According to the literature [69–73], the mutual dissolution of isomorphous $\text{Cr}_3\text{P}(\text{s})$ and $\text{Fe}_3\text{P}(\text{s})$, $\text{Cr}_2\text{P}(\text{s})$ and $\text{Fe}_2\text{P}(\text{s})$, $\text{CrP}(\text{s})$ and $\text{FeP}(\text{s})$ to form Me_3P , Me_2P , and MeP in the formulas of $(\text{Cr,Fe})_3\text{P}$, $(\text{Cr,Fe})_2\text{P}$, and $(\text{Cr,Fe})\text{P}$, respectively, occur in the ternary Cr–Fe–P system. Based on thermodynamic descriptions of the binary Cr–P, Cr–Fe, and Fe–P systems, the gas phase; red P; liquid solution; solid solutions including BCC_A2, FCC_A1, Sigma, Me_3P , Me_2P , and MeP ; and stoichiometric compounds including $\text{CrP}_2(\text{s})$ and $\text{FeP}_2(\text{s})$ were considered stable in the ternary Cr–Fe–P system.

3.3.1. The Cr–Fe–P Phase Diagram

The phase equilibria of a variety of vertical sections of the Cr–Fe–P system were measured by Vogel and Kasten [32] by means of thermal analysis and microscopic analysis. Figure 7 shows the calculated vertical diagrams for the mass ratios of $m(\text{Fe}):m(\text{Cr}) = 1:9$, $2:8$, $4:6$, $5:5$, $6:4$, $7:3$, $8:2$, and $9:1$ from previous assessment of the present optimization, compared to the experimental data. It can be seen that all experimental data are from the region of $\text{wt.\%P} < 28$ and are basically reproduced by both calculations. It is noted that the melting points of Me_2P optimized by the present study are approximately 50°C higher than those of the previous assessment, aiming at making more raised “Liquid + Me_2P ” liquidus boundaries for a better match with the experimental data of the higher-P region, as shown in the figure. Nevertheless, these high-P liquidus data could not be perfectly reproduced. This is probably due to non-neglectable vaporization of P from the melts at such a high P concentration region. As a consequence of the present optimization, the eutectic reaction $\text{Liquid} = \text{Me}_2\text{P} + \text{MeP}$ occurs in the lower-P composition, and the congruent melting points of MeP of the present study are $11\sim 84^\circ\text{C}$ higher than those of the previous assessment, depending on the ratio of $m(\text{Fe}):m(\text{Cr})$.

Figure 8 shows the calculated solubility of P in FCC_A1 and BCC_A2 Fe–Cr alloys between 700°C and 1140°C depending on the Cr content, compared to the experimental data [32,72]. According to the experiments of Kaneko et al. [72], the solubility of P in BCC_A2 Fe–Cr solution decreases continuously with increasing Cr concentration and decreasing temperature. These data are well reproduced by adding one binary model parameter ($L_{\text{Cr,P:Va}}^{\text{BCC_A2}} = -48,116 \text{ J/mol}$) for BCC_A1 of the Cr–P system. However, the calculation results of Miettinen and Vassilev for 900°C and 1000°C are not matched with the experimental data, as shown in Figure 8a. This discrepancy is due to the overestimated stability of the FCC_A1 phase, as shown in Figure 8b. After careful examination, it was found that Miettinen [20,21] made a mistake by excluding the FCC_A1 phase in the calculation of P solubility in BCC_A2 solution. That is why the FCC_A1 was not appearing in their phase diagram. To resolve the inconsistency, the interaction model parameter ($L_{\text{Cr,P:Va}}^{\text{FCC_A1}} = L_{\text{Cr,P:Va}}^{\text{BCC_A1}} = -70,000 \text{ J/mol}$) assessed by Miettinen [20,21] was optimized to be a less negative value ($L_{\text{Cr,P:Va}}^{\text{FCC_A1}} = L_{\text{Cr,P:Va}}^{\text{BCC_A1}} = -48,116 \text{ J/mol}$) in this study, as listed in Table 1.

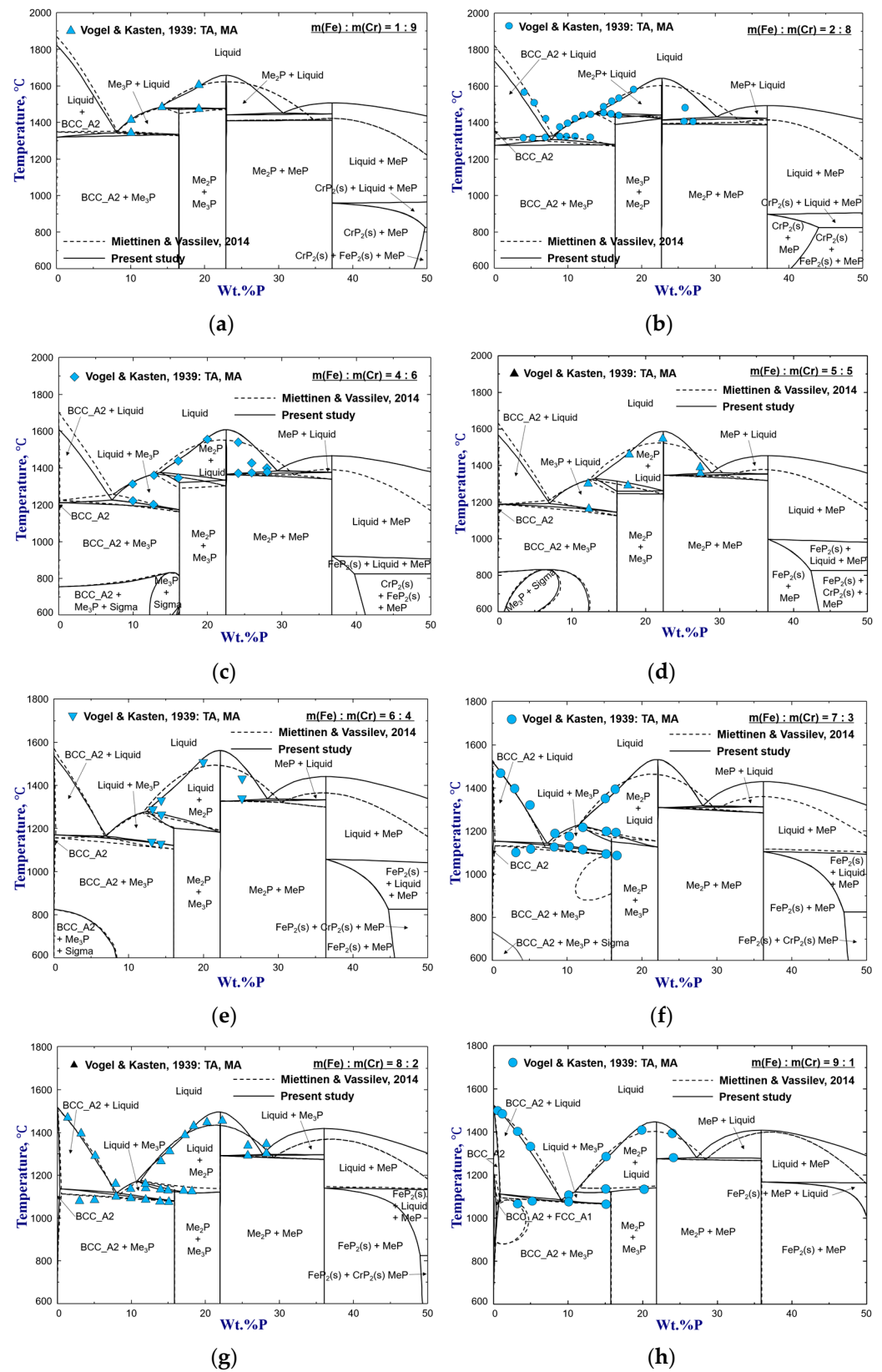


Figure 7. Calculated phase diagrams of the Cr–Fe–P system at the ratios of (a) $m(\text{Fe}):m(\text{Cr}) = 1:9$, (b) $m(\text{Fe}):m(\text{Cr}) = 2:8$, (c) $m(\text{Fe}):m(\text{Cr}) = 4:6$, (d) $m(\text{Fe}):m(\text{Cr}) = 5:5$, (e) $m(\text{Fe}):m(\text{Cr}) = 6:4$, (f) $m(\text{Fe}):m(\text{Cr}) = 7:3$, (g) $m(\text{Fe}):m(\text{Cr}) = 8:2$, and (h) $m(\text{Fe}):m(\text{Cr}) = 9:1$, compared to the experimental data [32].

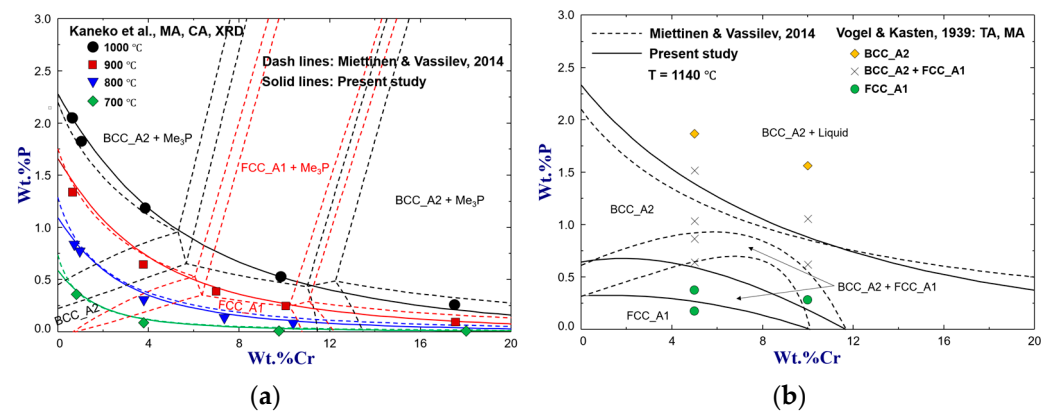


Figure 8. Calculated solubility of P in BCC_A2 and FCC_A1 solid solutions of the Cr–Fe–P system for (a) 700–1000 °C and (b) 1140 °C, compared to the experimental data [32,72].

The homogeneity range of the Me_3P and Me_2P solid solutions at 800 °C were investigated by Kaneko et al. [73] using XRD and chemical analysis. They found a complete mutual dissolution between Cr_2P and Fe_2P into Me_2P solid solution and dissolution of 10.5 wt.%Cr in Fe_3P to form Me_3P solution at this temperature. These experimental results and reported P solubility data in BCC_A2 solution are compared with the present calculation in Figure 9. The existing data are well accounted for by the calculation results. Based on the present model parameters, Me_3P , Me_2P , and MeP were calculated to be complete solid solutions at 800 °C, as shown in the figure.

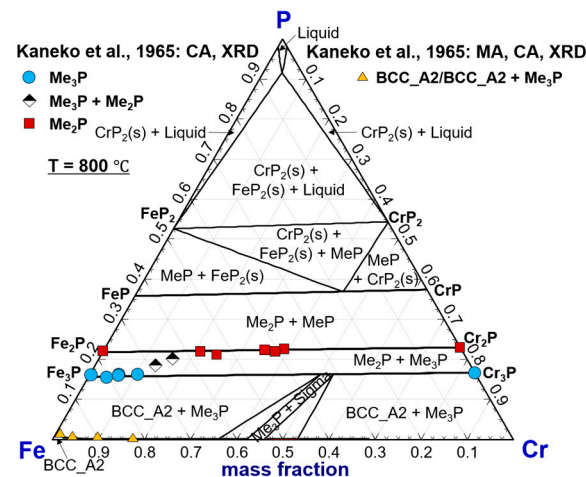


Figure 9. Calculated isothermal phase diagram of the Cr–Fe–P system at 800 °C, compared to the experimental data [72,73].

3.3.2. Thermodynamic Properties of the Cr–Fe–P Melts

The activity coefficient of P in molten Fe–Cr–P alloys at 1600 °C was studied by Froberg et al. [74] using the distribution method and Yamada and Kato [75] using the Knudsen effusion method. Figure 10 shows the calculated activity coefficient of P (1 wt.% standard state) against the P and Cr contents of the Fe–Cr–P melts at 1600 °C, compared to the experimental data. As can be seen from the figure, the calculated activities by Miettinen and Vassilev [21] deviate distinctly from the experimental data. It should be noted that Figure 10b was plotted in the form of “ $\ln \gamma_{\text{P}}^{\text{Cr}}$ against x_{Cr} ” by Miettinen and Vassilev [21]. That is why the data of Yamada and Kato [75] could still be reproduced despite a big discrepancy between the actual activity coefficient $f_{\text{P}}(\text{wt.}\%)$ and experimental results. In this study, these discrepancies left in the previous assessment were successfully resolved, as shown in Figure 10a,b.

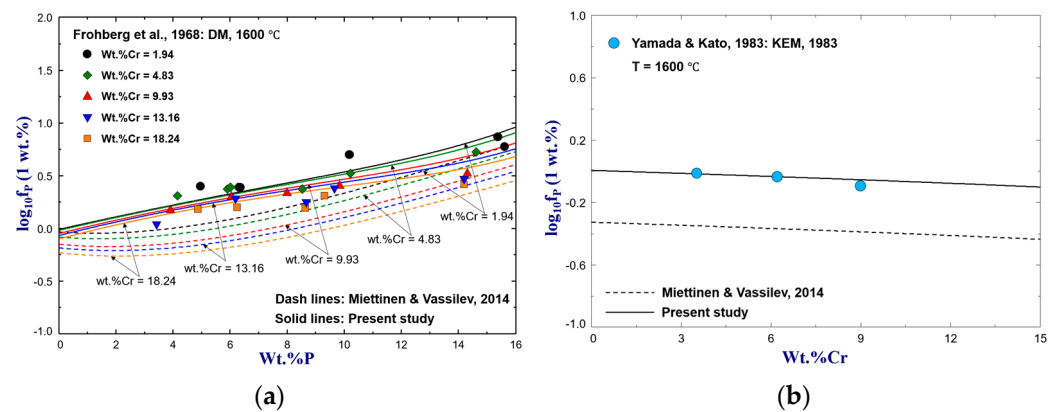


Figure 10. Calculated logarithmic activity coefficient of P (1 wt.% standard state) along with (a) wt.%P and (b) wt.%Cr in various molten Fe–Cr–P alloys at 1600 °C, compared to the experimental data [74,75].

Based on the present thermodynamic database, the activities of P(l), Fe(l), and Cr(l) in the wide composition and temperature ranges of liquid Cr–Fe–P solution were calculated and compared with the Knudsen effusion experiment data of Zaitsev et al. [76] in Figure 11. It is shown that most activity data for $a_{Cr(l)}$, $a_{Fe(l)}$, and $a_{P(l)}$ could be fitted except those of a_{Cr} at high Cr contents ($x_{Cr} = 0.50\sim 0.798$). After careful examination, it was found that these experimental data are contradicted by the Gibbs–Duhem equation. From a thermodynamic point of view, such discrepancies between the modeling results and the experimental results could not be resolved.

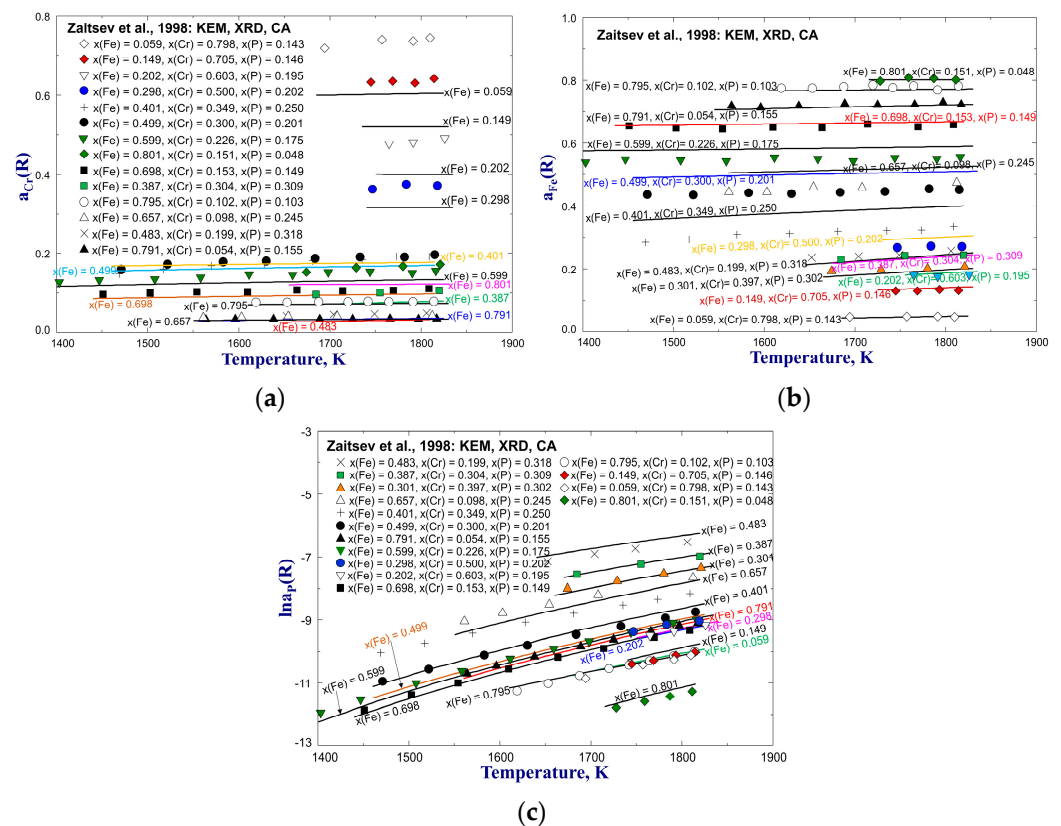


Figure 11. Calculated activities of (a) Cr, (b) Fe, and (c) P of liquid Cr–Fe–P solutions at various temperatures (pure liquid Cr(l), Fe(l), and P(l) as reference states), compared to the experimental data [76].

3.3.3. Improvement of Present Optimization Compared to Previous Assessments

The present optimization shows some improvements compared to previous assessments of the Cr–P system [20] and Cr–Fe–P system [21]. For the Cr–P system, the phase diagram of $x_P > 0.36$ was determined based on consistent descriptions of the liquid phase and all intermediate compounds ($\text{Cr}_3\text{P}(\text{s})$, $\text{Cr}_2\text{P}(\text{s})$, $\text{CrP}(\text{s})$, and $\text{CrP}_2(\text{s})$), and thermodynamic properties including heat capacity, standard enthalpy of formation, standard entropy, and Gibbs energy of Cr_3P and Cr_2P were optimized for more accurate reproduction of the experimental data. In the assessment of the Cr–Fe–P system by Miettinen and Vassilev [21], the phase equilibria of BCC_A2 and FCC_A1 solid solutions and the thermodynamic properties of the liquid solution were poorly determined. In the present optimization, more accurate descriptions were obtained by using fewer model parameters.

4. Predicted Phase Diagram of the Cr–Fe–P System

According to the optimized model parameters from the present study, the isothermal phase diagrams of 1000 °C and 1200 °C and liquid surface projection between 1000 °C and 2000 °C of the Cr–Fe–P system are predicted in Figures 12 and 13. As shown in Figure 12, Fe and Cr atoms can also substitute each other completely to form Me_2P and MeP solid solutions at 800 °C and 1200 °C. However, Me_3P starts to melt at wt.%Fe > 67 when the temperature rises up to 1200 °C. The natural logarithmic Henrian activity coefficient of P ($\ln\gamma_P^\circ$), which is of great importance to understand the thermodynamic behavior of P during production of the ferrochromium alloy, in the entire composition of Cr–Fe liquid solution at 1600 °C to 2100 °C is calculated in Figure 14.

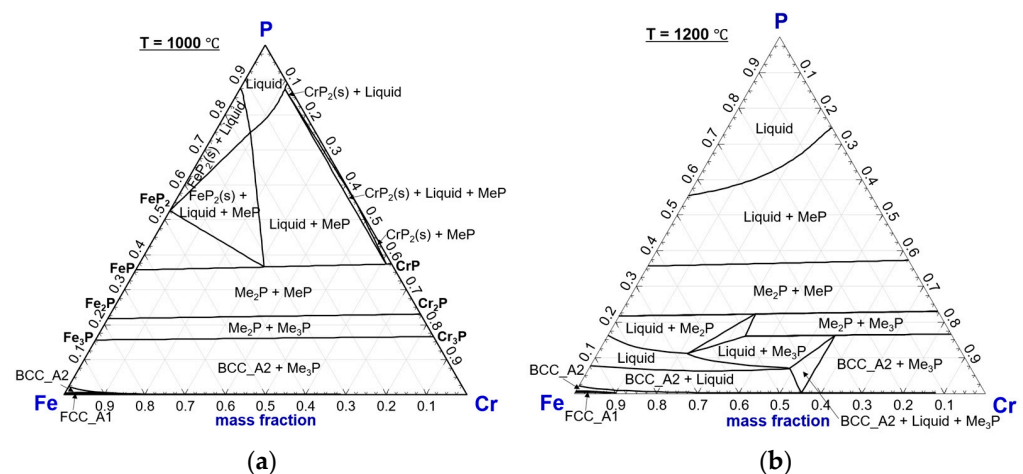


Figure 12. Predicted isothermal sections of the Cr–Fe–P system of (a) 1000 °C and (b) 1200 °C.

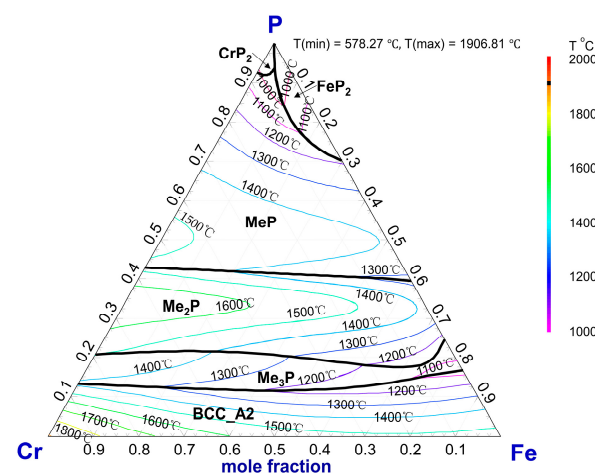


Figure 13. Predicted liquid surface projection of the Cr–Fe–P system between 1000 °C and 2000 °C.

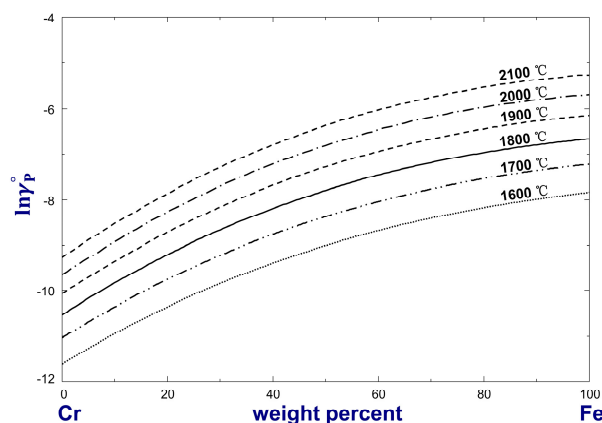


Figure 14. Predicted Henrian activity coefficient of P (γ_P^o) in the Cr–Fe melts at 1600 °C to 2100 °C.

5. Conclusions

Thermodynamic optimization of the binary Cr–P and ternary Cr–Fe–P systems in the entire composition range was performed based on the critical evaluation of the phase equilibria and thermodynamic properties data. The modified quasichemical model and compound energy formalism were used to describe the liquid and solid solutions, respectively. The CrP(s) and CrP₂(s) compounds were taken into account for the first time in the present thermodynamic modeling. The thermodynamic properties of Cr₃P(s), Cr₂P(s), CrP(s), and CrP₂(s) were carefully determined to reproduce reliable experimental data. In addition, the solubility of P in BCC_A2 and FCC_A1 phases and activity coefficient of P in Cr–Fe–P liquid solution were well optimized. Based on the present study, the discrepancies left in previous thermodynamic assessments of the Cr–P system and Cr–Fe–P system have been resolved with fewer model parameters. Any phase diagrams and thermodynamic properties within the Cr–Fe–P system can be predicted from the present thermodynamic database.

Author Contributions: Conceptualization, Z.Y.; Methodology, I.-H.J.; Investigation, Z.Y. and S.C.; Resources, Z.L. and S.C.; Data curation, Z.Y.; Writing—original draft, Z.Y.; Writing—review and editing, Z.J.; Visualization, Z.L.; Supervision, Z.J. and I.-H.J.; Funding acquisition, Z.Y. and Z.J. All authors have read and agreed to the published version of the manuscript.

Funding: This research was funded by the Program of Introducing Talents of Discipline to Universities, grant number B21001; National Natural Science Foundation of China, grant number 52204338; and Natural Science Foundation of Liaoning, grant number 2023-MSBA-047.

Data Availability Statement: The original contributions presented in the study are included in the article, further inquiries can be directed to the corresponding authors.

Conflicts of Interest: The authors declare no conflicts of interest.

Abbreviations

TA—Thermal Analysis; MGA—Metallographic Analysis; KEM—Knudsen Effusion Method; MSA—Mass Spectrometry Analysis; DSC—Differential Scanning Calorimetry; MLE—Mass Loss Effusion; XRD—X-ray Diffraction; VTM—Vapor Tension Measurement; MA—Microscopic Analysis; CA—Chemical Analysis; DM—Distribution Method.

References

1. Xu, T.; Yao, J.; Zhuo, L.; Jie, Z. Tuning non-isothermal crystallization kinetics between Fe₂₀Co₂₀Ni₂₀Cr₂₀(P_{0.45}B_{0.2}C_{0.35})₂₀ high-entropy metallic glass and the predecessor Fe₇₅Cr₅P₉B₄C₇ metallic glass. *Metals* **2023**, *13*, 1624. [\[CrossRef\]](#)
2. Li, B.; Lin, A.; Wu, X.; Zhang, Y.; Gan, F. Electrodeposition and characterization of Fe–Cr–P amorphous alloys from trivalent chromium sulfate electrolyte. *J. Alloys Compd.* **2008**, *453*, 93–101. [\[CrossRef\]](#)

3. Das, S.; Seol, J.B.; Kim, Y.C.; Park, C.G. Microscopic analysis of Fe–Cr alloy produced by single roll strip casting. *Mater. Sci. Technol.* **2011**, *27*, 1461–1464. [\[CrossRef\]](#)
4. Zorc, M.; Zorc, B.; Medved, J.; Nagode, A. A preliminary study of new experimental low-cost Fe–P-based and Mn–Fe–P-based brazing filler metals for brazing of non-alloy and low-alloy steels. *Metals* **2023**, *13*, 1513. [\[CrossRef\]](#)
5. Lu, S.; Chen, X.; Zheng, Q. Effects of the substitution of B and C for P on magnetic properties of FePCB amorphous alloys. *Metals* **2024**, *14*, 757. [\[CrossRef\]](#)
6. Andersson, J.O.; Sundman, B. Thermodynamic properties of the chromium–iron system. *CALPHAD* **1987**, *11*, 83–92. [\[CrossRef\]](#)
7. Chart, T.; Putland, F.; Dinsdale, A. Calculated phase equilibria for the chromium–iron–nickel–silicon system. I. Ternary equilibria. *Calphad* **1980**, *4*, 27–46. [\[CrossRef\]](#)
8. Hertzman, S.; Sundman, B. A thermodynamic analysis of the iron–chromium system. *Calphad* **1982**, *6*, 67–80. [\[CrossRef\]](#)
9. Lee, B.J. Revision of thermodynamic descriptions of the iron–chromium and iron–nickel liquid phases. *Calphad* **1993**, *17*, 251–268.
10. Xiong, W.; Hedström, P.; Selleby, M.; Odqvist, J.; Thuvander, M.; Chen, Q. An improved thermodynamic modeling of the Fe–Cr system down to zero kelvin coupled with key experiments. *Calphad* **2011**, *35*, 355–366. [\[CrossRef\]](#)
11. Spencer, P.; Kubaschewski, O. A Thermodynamic assessment of the Fe–P system. *Arch. Eisenhüttenwes.* **1978**, *49*, 225–228.
12. Gustafson, P. *Internal Report IM-2549*; Swedish Institute for Metals Research: Stockholm, Sweden, 1990.
13. Shim, J.H.; Oh, C.S.; Lee, D.N. Thermodynamic properties and calculation of phase diagram of the Fe–P system. *J. Korean. Inst. Met. Mater.* **1996**, *34*, 1385–1393.
14. Ohtani, H.; Hanaya, N.; Hasebe, M.; Teraoka, S.I.; Abe, M. Thermodynamic analysis of the Fe–Ti–P ternary system by incorporating first-principles calculations into the CALPHAD approach. *Calphad* **2006**, *30*, 147–158. [\[CrossRef\]](#)
15. Cao, Z.M.; Wang, K.P.; Qiao, Z.Y.; Du, G.W. Thermodynamic reoptimization of the Fe–P system. *Acta Phys. Chim. Sin.* **2012**, *28*, 37–43.
16. Cao, Z.M.; Xie, W.; Wang, K.P.; Niu, C.J.; Du, G.W.; Qiao, Z.Y. Thermodynamic optimization of the Al–Fe–P ternary system. *Acta Phys. Chim. Sin.* **2013**, *29*, 2148–2156.
17. Bernhard, M.; Kang, Y.B.; Presoly, P.; Gheribi, A.E.; Bernhard, C. Critical evaluation and thermodynamic modeling of the Fe–P and Fe–C–P system. *Calphad* **2020**, *70*, 101795. [\[CrossRef\]](#)
18. Cui, S.; Jung, I.-H. Thermodynamic modeling of the Cu–Fe–Cr and Cu–Fe–Mn systems. *Calphad* **2017**, *56*, 241–259. [\[CrossRef\]](#)
19. You, Z.M.; Jung, I.-H. Critical evaluation and optimization of the Fe–P system. *Metall. Mater. Trans. B* **2020**, *51B*, 3108–3129. [\[CrossRef\]](#)
20. Miettinen, J. Thermodynamic description of Cr–P and Fe–Cr–P systems at low phosphorus contents. *Calphad* **1999**, *23*, 141–154. [\[CrossRef\]](#)
21. Miettinen, J.; Vassilev, G. Thermodynamic description of ternary Fe–X–P Systems. Part 1: Fe–Cr–P. *J. Phase Equilib. Diffus.* **2014**, *35*, 458–468. [\[CrossRef\]](#)
22. Bale, W.; Chartrand, P.; Degterov, S.A.; Eriksson, G.; Hack, K.; Mahfoud, R.B.; Petersen, S. FactSage thermochemical software and databases. *Calphad* **2002**, *26*, 189–228. [\[CrossRef\]](#)
23. Dinsdale, T. SGTE data for pure elements. *Calphad* **1991**, *15*, 317–425. [\[CrossRef\]](#)
24. Inden, G. *Project Meeting CALPHAD V*; Max–Planck–Inst, Eisenforschung: Dusseldorf, Germany, 1976; Volume 111.
25. Hillert, M.; Jarl, M. A model for alloying in ferromagnetic metals. *Calphad* **1978**, *2*, 227–238. [\[CrossRef\]](#)
26. Hillert, M. The Compound Energy Formalism. *J. Alloys Compd.* **2001**, *320*, 161–176. [\[CrossRef\]](#)
27. Pelton, A.D.; Degterov, S.A.; Eriksson, G.; Robelin, C.; Dessureault, Y. The Modified Quasichemical Model I–binary solutions. *Metall. Mater. Trans. B* **2000**, *31*, 651–659. [\[CrossRef\]](#)
28. Pelton, A.D.; Chartrand, P. The Modified Quasi–chemical Model: Part II. Multicomponent solutions. *Metall. Mater. Trans. A* **2001**, *32*, 1355–1360. [\[CrossRef\]](#)
29. Huang, W. An assessment of the Fe–Mn system. *Calphad* **1989**, *13*, 243–252. [\[CrossRef\]](#)
30. Arstad, O.; Nowotny, H. X-ray investigation of the system Mn–P. *Z. Phys. Chem.* **1937**, *38*, 356–358.
31. Nowotny, H.; Henglein, E. Investigation of the system Cr–P. *Z. Anorg. Allg. Chem.* **1938**, *239*, 14–16. [\[CrossRef\]](#)
32. Vogel, R.; Kasten, G.W. The system iron–chromium–phosphorus. *Arch. Eisenhüttenwes.* **1939**, *12*, 387–391. [\[CrossRef\]](#)
33. Faller, F.E.; Biltz, W. On phosphides of tungsten, molybdenum and chromium. *Z. Anorg. Allg. Chem.* **1941**, *248*, 209–228. [\[CrossRef\]](#)
34. Schönberg, N. An X-ray investigation of transition metal phosphides. *Acta Chem. Scand.* **1954**, *8*, 226–239. [\[CrossRef\]](#)
35. Lundström, T. A ternary sigma phase in the system Cr–Ni–P. *Acta Chem. Scand.* **1962**, *16*, 149–154. [\[CrossRef\]](#)
36. Rundquist, S. X-ray investigation of the ternary system Fe–P–B. Some features of the systems Cr–P–B, Mn–P–B, Co–P–B and Ni–P–B. *Acta Chem. Scand.* **1962**, *16*, 1–19. [\[CrossRef\]](#)
37. Owusu, M.; Javad, H.; Lundström, T.; Rundquist, S. Crystallographic studies of Cr₃P and of the solid solution of hydrogen in Zr₃P. *Phys. Scr.* **1972**, *6*, 67–70. [\[CrossRef\]](#)
38. Aronsson, B.; Lundström, T.; Rundquist, S. Borides, silicides and phosphides: A critical review of their preparation, properties and crystal chemistry. *Acta Crystallogr.* **1966**, *20*, 323–324.
39. Lundström, T. Preparation and crystal chemistry of some refractory borides and phosphides. *Ark. Kemi* **1969**, *31*, 227–266.
40. Baurecht, H.E.; Boller, H.; Nowotny, H. X-ray investigation in the ternary system Cr–P–C, Cr–As–C and Cr–P–B. *Monatsh. Chem.* **1971**, *102*, 373–384. [\[CrossRef\]](#)

41. Roy–Montreuil, J.; Deyris, B.; Michel, A.; Rouault, A.; l’Heritier, P.; Nylund, A.; Senateur, J.P.; Fruchart, R. New MM’P and MM’As ternary compounds, metallic interactions and structures. *Mater. Res. Bull.* **1972**, *7*, 813–826. [\[CrossRef\]](#)
42. Chun, H.K.; Carpenter, G.B. Redetermination of the crystal structures of Cr₁₂P₇. *Acta Crystallogr. B* **1979**, *35*, 30–33. [\[CrossRef\]](#)
43. Maaref, S.; Madar, R.; Chaudouet, P.; Senateur, J.P.; Fruchart, R. Crystal chemistry of M₁₂P₇ phases in relation with the M₂P phosphides. *J. Solid State Chem.* **1981**, *40*, 131–135. [\[CrossRef\]](#)
44. Myers, C.E.; Kisacky, G.A.; Klingert, J.K. Vaporization behavior of chromium phosphides. The solid two–phase regions CrP–Cr₁₂P₇, Cr₁₂P₇–Cr₃P, and Cr₃P–Cr. *J. Electrochem. Soc.* **1985**, *132*, 236–238. [\[CrossRef\]](#)
45. Zaitsev, A.I.; Dobrokhotova, Z.V.; Litvina, A.D.; Elizarova, T.A.; Mogutnov, B.M. Thermodynamic properties of chromium phosphides. *Inorg. Mater.* **1995**, *31*, 1371–1380.
46. Granger, A. On the phosphides of chromium and manganese. *Compt. Rend.* **1897**, *124*, 190–191.
47. Granger, A. A contribution to the study of metallic phosphides. *Ann. Chim. Phys.* **1898**, *14*, 5–90.
48. Maronneau, G. On the preparation of phosphides of nickel, cobalt and chromium. *Compt. Rend.* **1900**, *130*, 656–658.
49. Diekmann, T.; Hanf, O. On some arsenides and phosphides of chromium. *Z. Anorg. Chem.* **1914**, *86*, 291–295.
50. Ripley, R.L. The preparation and properties of some transition phosphides. *J. Less–Common Met.* **1962**, *4*, 496–503. [\[CrossRef\]](#)
51. Rundquist, S. Phosphides of the B31(MnP) structure type. *Acta Chem. Scand.* **1962**, *16*, 287–292. [\[CrossRef\]](#)
52. Boller, H.; Nowotny, H. Crystallochemical investigations of monophosphides and monoarsenides in the systems: Ti–(Cr, Mo, W)–(P, As). *Monatsh. Chem.* **1965**, *96*, 852–862. [\[CrossRef\]](#)
53. Rundquist, S.; Nawapong, P.C. Crystal structure refinements of some MnP–type phosphides. *Acta Chem. Scand.* **1965**, *19*, 1006–1008. [\[CrossRef\]](#)
54. Selte, K.; Kjekshus, A.; Andresen, A.F. Structural and magnetic properties of CrP. *Acta Chem. Scand.* **1972**, *26*, 4188–4190. [\[CrossRef\]](#)
55. Selte, K.; Kjekshus, A. On phase transitions between the MnP and NiAs type structures. *Acta Chem. Scand.* **1973**, *27*, 3195–3206. [\[CrossRef\]](#)
56. Selte, K.; Hjersing, H.; Kjekshus, A.; Andresen, A.F.; Fischer, P. Magnetic structures and properties of CrP_{1–x}As_x. *Acta Chem. Scand.* **1975**, *29*, 695–698. [\[CrossRef\]](#)
57. Jeitschko, W.; Donahue, P.C. High–pressure CrP₂ and CrAs₂ with OsGe₂–type structure and crystal chemistry of transition metal dipnictides. *Acta Crystallogr. B* **1973**, *29*, 783–789. [\[CrossRef\]](#)
58. Jeitschko, W.; Donahue, P.C. The high pressure synthesis, crystal structure, and properties of CrP₄ and MoP₄. *Acta Crystallogr. B* **1972**, *28*, 1893–1898. [\[CrossRef\]](#)
59. Braun, D.J.; Jeitschko, W. On polyphosphides of chromium, manganese, ruthenium, and osmium. synthesis and crystal structure of RuP₄ and OsP₄. *Z. Anorg. Allg. Chem.* **1978**, *445*, 157–166. [\[CrossRef\]](#)
60. Venkatraman, M.; Neumann, J.P. The Cr–P (chromium–phosphorus) system. *J. Phase Equilib.* **1990**, *11*, 430–434. [\[CrossRef\]](#)
61. Fruchart, R.; Roger, A.; Senateur, J.P. Crystallographic and magnetic properties of solid solutions of the phosphides M₂P, M = Cr, Mn, Fe, Co, and Ni. *J. Appl. Phys.* **1969**, *40*, 1250–1257. [\[CrossRef\]](#)
62. Zaitsev, A.I.; Dobrokhotova, V.; Litvina, A.D.; Shelkova, N.E.; Mogutnov, B.M. Thermodynamic properties of chromium–phosphorus melts. *Inorg. Mater.* **1996**, *32*, 474–480.
63. Glaum, R.; Gruhn, R. On the chemical vapor transport of chromium and manganese monophosphide. Experimental results and thermochemical calculations. *Z. Anorg. Allg. Chem.* **1989**, *573*, 24–42. [\[CrossRef\]](#)
64. Schlesinger, M.E. The thermodynamic properties of phosphorus and solid binary phosphides. *Chem. Rev.* **2002**, *102*, 4267–4302. [\[CrossRef\]](#) [\[PubMed\]](#)
65. Pogorelyi, V.I. Activity of phosphorus in the system chromium–phosphorus. *Metall. Koksokhim.* **1974**, *39*, 8–12.
66. Kubaschewski, O.; Alcock, C.B. *Metallurgical Thermochemistry*, 5th ed.; Pergamon Press: Oxford, UK, 1979; Volume 24, pp. 1–462.
67. Nagai, T.; Miyake, M.; Kimura, H.; Maeda, M. Determination of Gibbs free energy of formation of Cr₃P by double Knudsen cell mass spectrometry. *J. Chem. Thermodyn.* **2008**, *40*, 471–475. [\[CrossRef\]](#)
68. Pogorelyi, V.I.; Gasik, M.I. Thermodynamics of the chromium–phosphorus system. *Proizvod. Ferrospl.* **2012**, *3*, 31–36.
69. Goto, M.; Tange, H.; Tokunaga, T.; Fujii, H.; Okamoto, T. Magnetic properties of the (Fe_{1–x}M_x)₃P compounds. *Jpn. J. Appl. Phys.* **1977**, *16*, 2175–2179. [\[CrossRef\]](#)
70. Thadani, P.; Toth, L.E.; Zbasnik, J. Low temperature heat capacities of transition metal phosphides. *J. Phys. Chem. Solids* **1975**, *36*, 987–991. [\[CrossRef\]](#)
71. Sjöström, J.; Jarlborg, T. Band structures and magnetic properties in the iron phosphide compounds FeMnP, FeCrP and FeVP. *J. Magn. Magn. Mater.* **1991**, *98*, 85–91. [\[CrossRef\]](#)
72. Kaneko, H.; Nishizawa, T.; Tamaki, K.; Tanifuji, A. Solubility of phosphorus in α and γ–iron. *Nippon. Kinzoku Gakkai–Si* **1965**, *29*, 166–170.
73. Kaneko, H. Phosphide–phases in ternary alloys of iron, phosphorus and other elements. *J. Jpn. Inst. Met.* **1965**, *29*, 159–165. [\[CrossRef\]](#)
74. Froberg, M.; Elliott, J.; Hadrys, H. Contribution to study of thermodynamics of complex solutions shown by example homogeneous Fe–Cr–P–C melts. *Arch. Eisenhutten.* **1968**, *39*, 587–593.

75. Yamada, K.; Kato, E. Effect of dilute concentrations of Si, Al, Ti, V, Cr, Co, Ni, Nb and Mo on the activity coefficient of P in liquid iron. *Trans. Iron Steel Inst. Jpn.* **1983**, *23*, 51–55. [[CrossRef](#)]
76. Zaitsev, A.I.; Shelkova, N.E.; Mogutnov, B.M. Thermodynamic properties of iron–chromium–phosphorus melts. *Russ. J. Inorg. Chem.* **1997**, *42*, 1567–1573.

Disclaimer/Publisher’s Note: The statements, opinions and data contained in all publications are solely those of the individual author(s) and contributor(s) and not of MDPI and/or the editor(s). MDPI and/or the editor(s) disclaim responsibility for any injury to people or property resulting from any ideas, methods, instructions or products referred to in the content.